Journal of Applied Physics

Hot phonon effects and Auger recombination on 3 μm room temperature lasing in HgTe-based multiple quantum well diodes

Cite as: J. Appl. Phys. **132**, 073103 (2022); https://doi.org/10.1063/5.0098918
Submitted: 13 May 2022 • Accepted: 17 July 2022 • Published Online: 17 August 2022

A. A. Afonenko, D. V. Ushakov, A. A. Dubinov, et al.

Journal of Applied Physics ARTICLE scitation.org/journal/jap

Hot phonon effects and Auger recombination on 3 μm room temperature lasing in HgTe-based multiple quantum well diodes

Cite as: J. Appl. Phys. **132**, 073103 (2022); doi: 10.1063/5.0098918
Submitted: 13 May 2022 · Accepted: 17 July 2022 ·
Published Online: 17 August 2022

A. A. Afonenko,[1,a)] D. V. Ushakov,[1] A. A. Dubinov,[2,3] V. Ya. Aleshkin,[2,4] S. V. Morozov,[2,3] and V. I. Gavrilenko[2,4]

AFFILIATIONS

[1]Department of Radiophysics and Computer Technologies, Belarusian State University, 220030 Minsk, Belarus
[2]Institute for Physics of Microstructures, Russian Academy of Sciences, 603950 Nizhny Novgorod, Russia
[3]Department of Radiophysics, Lobachevsky State University, 603950 Nizhny Novgorod, Russia
[4]Advanced School of General and Applied Physics, Lobachevsky State University, 603950 Nizhny Novgorod, Russia

[a)]**Author to whom correspondence should be addressed:** afonenko@bsu.by

ABSTRACT

We propose an electrically pumped laser diode based on multiple HgTe quantum wells with band structure engineered for Auger recombination suppression. A model for accounting for hot phonons is developed for calculating the nonequilibrium temperature of electrons and holes. Using a comprehensive model accounting for carrier drift and diffusion, Auger recombination, and hot-phonon effects, we predict of lasing at $\lambda \sim 3\,\mu$m at room temperature in the 2.1 nm HgTe/$Cd_{0.85}Hg_{0.15}Te$ quantum well heterostructure. The output power in the pulse can reach up to 600 mW for 100 nanosecond-duration pulses.

I. INTRODUCTION

The radiation sources of wavelength around 3 μm in the atmospheric transparency window are of extreme importance for gas sensing applications, environmental control, and medical diagnostics due to fundamental absorption lines of different substances, for example, paramylon,[1] n-butanol, ethene, and ethylene oxide.[2] Laser sources with this wavelength are also required for lidar systems[3] and free space optical communication systems.[4]

Laser action with a wavelength around 3 μm was realized in semiconductor systems based on III–V (GaSb, InAs), IV–VI (PbS, PbSe), and II–VI compounds.[5–7] However, conventional interband laser diode designs require four and five component solid solutions,[6] which require the highest level of production and limit their distribution. Also, promising sources are quantum-cascade lasers (QCLs) consisting of layers of hundreds of layers and three-component III–V semiconductor solutions.[8–13] The use of a sequence of narrow- and wide-gap compounds on In(Ga)As/AlAs(Sb) makes it possible to increase the height of potential barriers in the conduction band up to 2 eV, which made it possible to develop indoor short-wavelength QCLs operating in the region of 2.6–3.5 μm.[12,14–16] However, the growth of a large number of layers is also associated with enormous technological difficulties.

In this regard, the sources based on CdHgTe with HgTe quantum wells (QWs) could be compelling. HgCdTe technology is well-developed and is used for the fabrication of IR detectors.[17,18] Earlier, lasers based on bulk CdHgTe layers (with optical[19] and electrical pumping[20,21]) and based on wide CdHgTe QWs with a significant cadmium content $x = 0.5$–0.34 (only with optical pumping[22–24]) were created. It is found that lasing is suppressed due to a highly increasing Auger 3D coefficient from 4.9×10^{-28} cm^6/s ($x = 0.5$) to 9×10^{-26} cm^6/s ($x = 0.34$) at 100 K with a decrease in the bandgap of active layers[24] in the 1.9–3.5 μm wavelength range. Estimated Auger 2D coefficient for QW structures increased from 2.1×10^{-16} cm^4/s ($x = 0.44$) to 9×10^{-14} cm^4/s ($x = 0.34$).

However, due to the progress in molecular beam epitaxy, the active region of HgCdTe-based emitters can be formed not only by bulk layers but also by arrays of the binary HgTe QWs. In such quantum well heterostructures, it is easier to achieve population

inversion as suggested earlier.[25] As shown in recent works,[26–28] when using HgTe active layers, it is possible to suppress Auger recombination. As a result, interest in this system of materials was revived, and with optical pumping, it was possible to observe stimulated emission at wavelengths of 3.7,[29] 2.8,[30] and 2.45 μm[31] at temperatures of 240, 250, and 300 K, respectively. Estimated Auger coefficient for QW structures emitted at $\lambda \approx 3.7\,\mu$m was 10^{-27} cm^6/s (3D) or 1.4×10^{-14} cm^4/s (2D).[29] Possibly, the large values of the lasing threshold and overestimation of the Auger recombination coefficient in Ref. 23 were also contributed by the low optical confinement in the structures.

The main factors that limit the temperature characteristics of mid-infrared (IR) semiconductor lasers are Auger recombination on the QWs, non-equilibrium carrier heating and Drude absorption of the free carriers. Although yet there is no experimental demonstration of injection lasers based on heterostructures with HgTe QWs, there are several theoretical proposals of diode laser aimed for mid-[25] and far-IR[32] operation as well as THz quantum-cascade laser[33] based on HgCdTe. In this work given, the experimental results demonstrating stimulated emission under optical pumping[29–31] and suppression of Auger recombination in HgTe QWs,[26,34] we investigate the feasibility of HgCdTe-based injection lasers. Considered laser design has active regions consisting of several 2.1-nm thick HgTe QWs separated by $Cd_xHg_{1-x}Te$ barriers. The QW width is selected to achieve the emission wavelength of 3 μm. Here, using a complex numerical model that takes into account the drift and diffusion of carriers in the barrier layers, carrier capture in the quantum wells, radiative and non-radiative recombination and heating of the active region, we show the possibility of generation at room temperature. We develop a model that accounts for hot phonons and show the essential influence of non-equilibrium heating of charge carriers on the output characteristics of lasers, especially for structures with deep QWs and low optical phonon energy.

II. STRUCTURE DESIGN

We consider the following multiple quantum well laser structure grown on a (013)-oriented n-GaAs substrate: 100 μm n-GaAs substrate/5 μm n-CdTe cladding/600 nm n-$Cd_xHg_{1-x}Te$ waveguide (x varies between 0.6 and 1)/active region (six–ten 2.1 nm HgTe QWs interleaved with 10 nm $Cd_{0.85}Hg_{0.15}Te$ barriers)/70 nm p-$Cd_xHg_{1-x}Te$ waveguide (x varies between 0.85 and 1.0)/3 μm p-CdTe cladding. The calculated parameters of each heterostructure layer are collected in Table I.

There were problems with CdHgTe technology of obtaining doping with acceptors with the desired profile and concentration

TABLE I. Parameters of heterostructure layers: layer number (No.), thickness (d), composition, doping, electron (μ_n) and hole (μ_p) mobilities, bandgap (E_g) and real part of the refractive index (n') for the ~3 μm wavelength. All the quantities are for 3D materials and temperature 300 K. In the graded-composition waveguide layers, the parameters vary linearly between their values in adjacent layers.

No.	d (nm)	Composition	Doping (cm^{-3})	μ_n ($\frac{cm^2}{V\ s}$)	μ_p ($\frac{cm^2}{V\ s}$)	E_g (eV)	n'
			Substrate				
1		GaAs	$n: 10^{18}$	2361	134	1.42	3.31
			n-cladding layer				
2	5000	CdTe	$n: 10^{17}$	111	36	1.49	2.71
			n-waveguide layers				
3	50	CdTe	$n: 5 \times 10^{17}$	40	16	1.49	2.7
4	50	graded					
5	400	$Cd_{0.6}Hg_{0.4}Te$	$n: 10^{17}$	197	36	0.71	2.86
6	50	graded					
7	30	$Cd_{0.9}Hg_{0.1}Te$	$n: 10^{18}$	30	11	1.26	2.74
8	10	graded					
9	10	$Cd_{0.85}Hg_{0.15}Te$	$n: 10^{16}$	523	73	1.15	2.78
			active region				
10	2.1	QW: HgTe	0	523	73	−0.14	5.14
11	10	$Cd_{0.85}Hg_{0.15}Te$	$n: 10^{16}$	523	73	1.15	2.78
			+ (5÷9) + 1/2 periods (two layers in period)				
			p-waveguide layers				
12	10	$Cd_{0.85}Hg_{0.15}Te$	$n: 10^{16}$	523	73	1.15	2.78
13	10	graded					
14	20	CdTe	$p: 5 \times 10^{17}$	40	16	1.49	2.71
15	30	CdTe	$p: 1 \times 10^{16}$	414	73	1.49	2.71
			p-cladding layer				
16	3000	CdTe	$p: 4 \times 10^{16}$	194	51	1.49	2.71
			Au contact layer				

for a long time. Recently, it was shown that the existing technologies of epitaxial growth make it possible to create p-CdTe with the concentration and hole distribution profile required in our work (Ref. 35 and references therein). The use of the (013) GaAs substrate orientation significantly increases the maximum possible hole concentration and sharpness of the doping profile.

Band structure parameters (bandgap, effective masses) of ternary and binary compounds were obtained from experimental and theoretical data using the approach of Refs. 36 and 37. Electron and hole mobilities were interpolated from the experimental data of Refs. 38 and 39. Infrared refractive index and absorption coefficient of the waveguide were calculated taking into account Drude and lattice absorption.[40–42] Internal optical losses and refractive index were calculated within the multioscillator Lorentz–Drude model including both phonon and free-carrier contributions.[40–42] Calculated absorption cross sections of the free electrons and holes were 1.7×10^{-17} and 1.2×10^{-16} cm^2, respectively. Quantum well depths for electrons and holes were calculated according to Refs. 36 and 43.

Refractive index was interpolated from Ref. 44 for the Cd content in the range of 0.18–1.0. During the interpolation, the background permittivity caused by the transitions involving L and X valleys was found analogously to Ref. 45. Resonant input of interband transitions for bulk semiconductor was calculated according to Ref. 46. At the same time, for HgTe, the experimental data are scarce. We did not find the direct measurements of the refractive index of HgTe in the mid-IR range. The available experimental works present the measurements of refractive index in the range of phonon absorption of 19–20 meV and photon energies above 1.5 eV.[47] Thus, in order to calculate the refractive index of HgTe QWs, we used a combination of the background permittivity extrapolated to $x = 0$ from the results obtained in Ref. 44 and resonance term related to step-function density of states caused by dimensional quantization. The obtained value of refractive index for HgTe QWs at $\lambda = 2.97\,\mu$m is equal to 5.14 (see Table I). It agrees with the value of ~4.6 obtained in Ref. 48, for HgTe(4 nm)/CdTe(2 nm) superlattice at the wavelength of its absorption edge equal to 6.7 μm. This refractive index is a weighted average composed of 2/3 of the refractive index of HgTe 5.6 and 1/3 of the refractive index of CdTe 2.71. Note that within the calculations of electromagnetic modes, we also take into account carrier induced refractive index change, which under conditions of injection decreases the refractive index to 4.8 (Fig. 1).

In order to reduce Auger recombination in the well, the mole composition of the barrier layers was chosen to be ~0.85, which corresponds to a refractive index of 2.78, which is slightly higher than the refractive index of CdTe 2.71. Because of the small change of refractive indices and small thickness of the core, the waveguide effect turned out to be very weak. Therefore, additional waveguide layers around the active region are required. In our calculations, we used $Cd_{0.6}Hg_{0.4}Te$ with 400 nm thickness and refractive index of 2.86 (see Fig. 1). Total calculated optical confinement factor is $\Gamma \approx 0.0018$ per QW. The suggested design also includes high $Cd_{0.9}Hg_{0.1}Te$ barrier placed between the active and waveguide layers to prevent parasitic interband recombination in the waveguide layer due to hole injection into it.

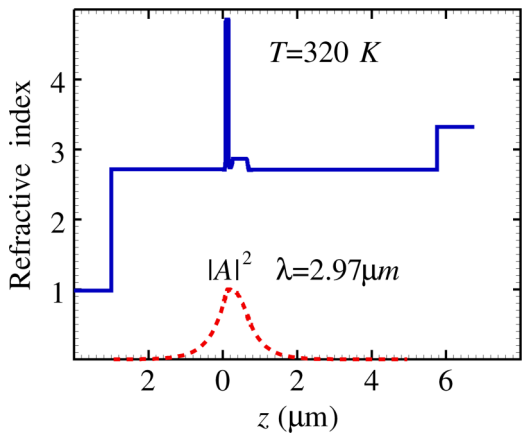

FIG. 1. Spatial distribution of the refractive index across the simulated heterostructure at $\lambda = 2.97\,\mu$m and the squared electric field of the ground TE mode. The total optical confinement factor of 8 quantum wells is $\Gamma = 0.014$, the effective refractive index is $n_{eff} = 2.78$.

The reflection coefficient of the output facet for the TE_0 mode was chosen equal to Fresnel reflection $r = 0.2$. The opposite facet was considered with a high reflection coating with a reflection coefficient $r = 0.9$.

III. THEORETICAL MODEL

This structure was simulated using a distributed drift-diffusion model based on one-dimensional (1D) Poisson's equation and continuity equations for electrons and holes with taking into account the carrier capture and escape processes.[49] Both radiative and Auger recombination were included in the model.

The band structure parameters were obtained from the eight-band $\mathbf{k} \cdot \mathbf{p}$ method.[36,37] Quantum well depths for electrons and holes were calculated according to Refs. 36 and 43. Carrier mobilities were interpolated from the experimental data of Ref. 38. The gain and spontaneous recombination were calculated in the model of direct innterband transitions with the broadening parameter of 5 meV. This broadening was included since the quantum well's width variation for molecular beam epitaxy of HgTe is ± 0.3 nm. Quantum-cascade lasers based on AlGaAs/GaAs with the similar errors in the grown exhibit lasing, confirming the broadening parameter is no more than 3 meV. We use the larger broadening parameter for HgTe/HgCdTe due to the lower effective mass.

An example of calculated band diagrams of structure with 8 QW and carrier distributions are shown in Fig. 2. In order to reduce optical losses, doping of most of the layers was selected to be below 10^{17} cm^{-3}. This results in a large ohmic resistance and a noticeable decline of the of quasi Fermi levels in the emitters. Gradient layers reduce the space charge region, while introduction of a wide-gap $Cd_{0.9}Hg_{0.1}Te$ blocking layer creates a barrier for the holes, preventing excitation of the waveguide. The series resistance of the laser structure was 1.3 Ω, cutoff voltage was 0.95 V. Thus, the bias voltage across the whole structure was 8–30 V depending on the current.

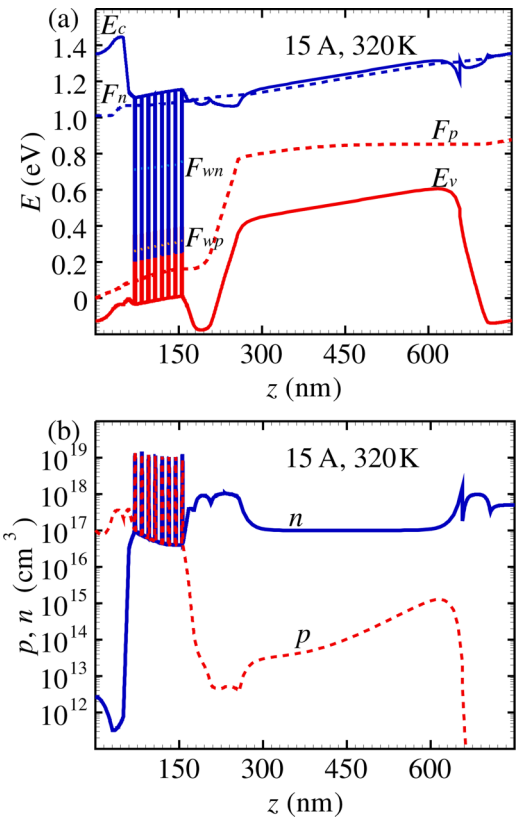

FIG. 2. (a) Band diagram and (b) distribution of carrier densities inside the 8 QW active region of the simulated heterostructure, calculated at 320 K, 15 A drive current [above the lasing threshold: photon density $S^{(2D)} = 1.25 \times 10^{11}\,\mathrm{cm}^{-2}$]. F_{wn}, F_{wp} (F_n, F_p) are the quasi-Fermi levels of localized (delocalized) carriers.

Distribution of the photon density across the resonator was found from the Bouguer–Lambert–Beer law.

Heating effects were taken into account by solving the 1D heat equation in the direction perpendicular to the heterostructure layers (we consider pulsed operation, when in-layer heat transfer during a pulse is negligible). We also included the temperature dependence of the bandgap in our model. In this work, the pulsed generation mode was studied. During the pulse, the effective size of heat spreading from a point source is $\sim 2\sqrt{\chi\tau}$. Assuming the pulse duration is $\tau = 100$ ns, the thermal diffusion length is 1.0–1.5 μm ($\chi = 0.03$–$0.05\,\mathrm{cm}^2/\mathrm{s}$ is the heat transfer coefficient). Therefore, the contact areas, including the heat sink, do not affect the generation processes. For active region size of 100 μm × 1 mm, the 1D heat equation along the normal to the plane of active layers is a sufficient approximation.

The self-consistent distributed model for calculating the electrophysical, optical, and thermal processes in injection lasers under pulse pumping is described in detail in Ref. 32. The model is based on quasi-stationary solutions for the photon density in the cavity. This is applicable here as the pump duration (100 ns) is much longer than the duration of the estimated transient process with photon density oscillations (~1–2 ns).

IV. AUGER RECOMBINATION

In our calculations of the interband recombination, we included both the radiative and Auger processes.[32,50–52] In this work, the coefficient of Auger recombination was calculated numerically. For a process involving two electrons and one hole, the coefficient C_{nnp} was found from the expression

$$C_{nnp} n^2 p = \frac{2\pi}{\hbar} \int\int\int \left\langle \left| V^2_{1234} \right| \right\rangle f_c(E_1) f_c(E_2) f_v(E_3) \times [1 - f_c(E_4)] \delta(E_1 + E_2 - E_3 - E_4) \times \frac{1}{2} \frac{2d\mathbf{k}_1}{(2\pi)^2} \frac{2d\mathbf{k}_2}{(2\pi)^2} \frac{d\mathbf{k}_3}{(2\pi)^2}, \quad (1)$$

where $\hbar$ is the reduced Planck constant, E_i and $\mathbf{k}_i$ are the energies and the wave vectors of the particles involved in the interaction, $f_c(E)$ and $f_v(E)$ are Fermi–Dirac functions for electrons and holes, n and p are the concentrations of electrons and holes,

$$\left\langle \left| V^2_{1234} \right| \right\rangle = \left(\frac{2\pi e^2}{4\pi\epsilon\epsilon_0} \right)^2 \times \frac{1}{4} \sum_{\alpha,\beta,\gamma,\delta} \left| \frac{V_{4\delta\,3\gamma,1\alpha\,2\beta}}{q_{13}} - \frac{V_{4\delta\,3\gamma,2\beta\,1\alpha}}{q_{23}} \right|^2, \quad (2)$$

is averaged square of the matrix element of the Coulomb interaction in a quasi-two-dimensional system, taking into account the exchange interaction, $q_{ij} = \sqrt{q^2_{\mathrm{scr}} + (\mathbf{k}_i - \mathbf{k}_j)^2}$, q_{scr} is the inverse screening length,

$$V_{4\delta\,3\gamma,1\alpha\,2\beta} = \int\int \psi^*_{c4\delta}(z_2) \psi^*_{v3\gamma}(z_1) \exp(-q_{13}|z_1 - z_2|) \times \psi_{c1\alpha}(z_1) \psi_{c2\beta}(z_2)\, dz_1\, dz_2, \quad (3)$$

are the matrix element of the Coulomb interaction of selected states. The indices α, β, γ, δ number the initial and final states that are doubly degenerate in the electron spin, $\psi(z)$ are dependences of wave functions on the coordinate z. The wavefunctions and their energies were found by the 8-band $\mathbf{k} \cdot p$ method.[36,37] The inverse screening length was calculated as for a 2D system of electrons and holes,

$$q_{\mathrm{scr}} = \frac{e^2}{2\epsilon\epsilon_0} \left(\frac{\partial n}{\partial F_{wn}} - \frac{\partial p}{\partial F_{wp}} \right). \quad (4)$$

Here, F_n and F_p are quasi Fermi levels for electrons and holes.

The coefficients of Auger recombination involving two holes and one electron C_{npp} were calculated by the formulas (1)–(3) with interchange $c \leftrightarrow v$.

The states of the continuum were calculated in a limited volume. Therefore, from a mathematical point of view, all states were discrete (2D) and Eq. (1) was applicable. The transition to 3D

was carried out by increasing the size of the analyzed continuum. In the work, the size of continuum was 20 nm and it was limited by the time for calculating the resulting Auger coefficient. It was necessary to sum the contributions from all states, and the number of states increases with increasing size of continuum.

For the analyzed quantum well HgTe/$Cd_{0.85}Hg_{0.15}Te$ 2.1 nm wide for 300 K, the coefficients of Auger recombination for electrons $C_{nnp} = 9.2 \times 10^{-16}$ cm^4/s and for holes $C_{npp} = 3.8 \times 10^{-15}$ cm^4/s. The level of excitation was taken close to the threshold. The summary coefficient of 4.7×10^{-15} cm^4/s is a bit higher than typical values $1 - 4 \times 10^{-15}$ cm^4/s for type-I and type-II III–V quantum wells emitting in the same spectral range.[7]

Resonant transitions with a small change in wave vectors ($< q_{scr}$) make a significant contribution to the recombination. In this case, the final high-energy state can be a continuum state. For example, for transitions involving two electrons and one hole, this contribution is about half of the resulting coefficient, while for a nonresonant transition with the participation of localized electrons only in the first subband, the recombination Auger coefficient is $C_{nnp} = 4.4 \times 10^{-16}$ cm^4/s. Auger recombination for transitions involving two holes and one electron is determined mainly by resonant transitions, and the corresponding coefficient is 4 times higher than the value for a process involving two electrons and one hole. This differs from the Auger calculations of recombination without taking into account the continuum states, when CCCH process with scattering of two electrons and one heavy hole is the most probable among different types of Auger processes in narrow-gap materials.[28] Quantitatively, the obtained values of the resulting recombination Auger coefficient $C = C_{nnp} + C_{npp} = 4.7 \times 10^{-15}$ cm^4/s for $n = p$ is smaller than in calculations,[28] where only transitions involving localized electrons and holes were taken into account ($C_{nnp} = 1.2 \times 10^{-14}$ cm^4/s). However, the exchange interaction, which reduces the recombination Auger coefficient, was not taken into account in Ref. 28.

Verification of the coefficients of Auger recombination with the experimental data of Ref. 29 has been carried out. For $Cd_{0.08}Hg_{0.92}Te/Cd_{0.8}Hg_{0.2}Te$ quantum wells with thickness of 2.7 nm ($\lambda \approx 3.7\,\mu$m), the measured value at an external temperature of 250 K and an electron temperature of 400 K and the charge carrier concentration of 1.2×10^{12} cm^{-2} is $C^{3D} \approx 10^{-27}$ cm^6/s. According to our calculations, based on formulas (1)–(3) for a temperature of 400 K $C^{3D} = C^{2D}d^2 = 6.5 \times 10^{-28}$ cm^6/s.

V. HOT PHONON EFFECT

One of the mechanisms limiting the output power of semiconductor lasers is nonequilibrium heating of electrons in quantum wells.[53,54] "Hot" electrons appear in the active region through the process of their capture from barrier regions to localized levels and subsequent thermalization to the lower levels of the quantum well. Also, Auger recombination causes heating of the carriers.[55] Electrons and holes lose energy by emitting optical phonons. Due to the high concentration of charge carriers and the high frequency of collisions, the temperatures of "hot" electrons and holes can be considered to be approximately equal.[55] The accumulation of optical phonons significantly reduces the rate of energy dissipation.[55] The processes of relaxation of the electron and hole temperature to the "hot" phonon temperature are faster than the equilibration of the "hot" phonon temperature and the lattice temperature. Therefore, it is possible to consider the temperature of electrons and holes equal to the temperature of "hot" phonons,

$$N_{ph} = \frac{1}{\exp\left(\frac{\hbar\omega_{LO}}{k_B T}\right) - 1}. \quad (5)$$

Here, N_{ph} and $\hbar\omega_{LO}$ are the number and the energy of optical phonons, respectively. This approximation greatly simplifies the analysis compared to the detailed model of Ref. 55, where a quantitative calculation of the electron–phonon scattering probabilities is required.

The balance of "hot" phonons N_{ph} was estimated analogously to Refs. 56 and 57 from the equation

$$\frac{dN_{ph}}{dt} = -\frac{N_{ph} - N_{ph\,0}}{\tau_{ph}} + \eta_{ph}\frac{RE_{gb} - (R_{st} + R_{sp})\hbar\omega}{\rho_{ph}\hbar\omega_{LO}}. \quad (6)$$

Here, $N_{ph\,0}$ is the equilibrium occupation numbers of phonon modes, τ_{ph} is the lifetime of phonon modes, which takes into account the decay of optical phonons into acoustic phonons, scattering processes on interface roughness, etc. R is the rate of electron (hole) injection in a QW, E_{gb} is the bandgap energy of the barrier layers, R_{st} and R_{sp} are the rates of stimulated and spontaneous recombination, respectively, $\hbar\omega$ is the energy of emitted photons, ρ_{ph} is the density of phonon modes, effectively interacting with electrons and holes. η_{ph} is the portion of emitted phonons, which fall into the modes involved in thermalization of the carriers near the bottom of the band.

According to Eq. (6), the number of emitted phonons is determined by the ratio of the energy of particles entering the active region reduced by the energy carried away by radiation to the energy of one phonon. For the barrier bandgap of 1.15 eV and the phonon energy of 18 meV, the capture of an electron–hole pair into a quantum well leads to the emission of about 40 phonons for radiative recombination ($\hbar\omega = 0.41$ eV) and about 64 phonons for nonradiative (Auger) recombination of electron–hole pair in a quantum well. Also, we neglected that the fast intra-subband relaxation can also generate acoustic phonons. Thus, the described method gives an upper bound for the nonequilibrium phonon temperature.

For the estimates, one can consider an ensemble of the "hot" phonons consisting of all the phonons with wavevector smaller than the highest possible value of the wavevector of the emitted phonons,

$$q_{ph} \le |\mathbf{k}_2| + |\mathbf{k}_1| \approx 2|\mathbf{k}_2|, \quad (7)$$

where $\mathbf{k}_2$ and $\mathbf{k}_1$ are the wavevectors of the initial and final states of the electron, respectively. Approximation is true for the transitions of electrons with the energy $E(k) - E(0) \gg \hbar\omega_{LO}$. Scattering with a subband change is less probable than scattering inside one subband. Therefore, we assume that first carriers relax inside a subband to its bottom and then they move to the states of the subband with lower energy, as shown in Fig. 3. In this case, the

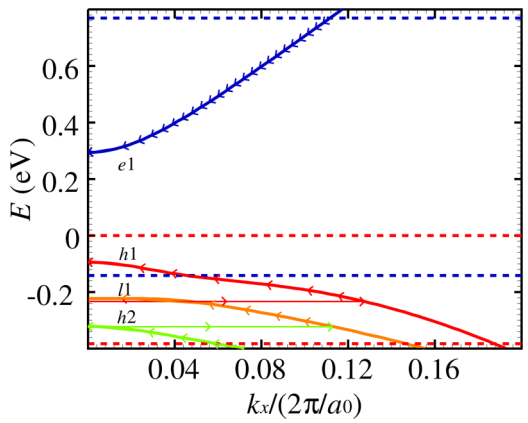

FIG. 3. Dispersion of electrons and holes in the [013] direction in a 2.1 nm thick $HgTe/Cd_{0.85}Hg_{0.15}Te$ quantum well. Horizontal lines show the energies of the edges of the QW and the barrier layers of the conduction band (blue dashed lines) and the valence band (red dashed lines). Arrows show the transitions of charge carriers associated with the emission of optical phonons.

density of phonon modes can be obtained after averaging the square of the wavevector of the current carrier with regard to its energy,

$$\rho_{\rm ph} = \frac{\langle k^2 \rangle_E}{\pi^2}. \tag{8}$$

Here, the fraction of emitted phonons falling into localized phonon modes is considered to be $\eta_{\rm ph} = 1$.

The described method for estimating the nonequilibrium temperature provides underestimated values for overheating, since it does not take into account the uneven distribution of emitted phonons along the wavevectors and the selective interaction of electrons and holes with phonons.

In order to find the distribution of emitted phonons along the wavevectors, we can write the probability of electron transition by emitting optical phonons,

$$\omega_q = \frac{2\pi}{\hbar} \left| V_q^2 \right| \delta(E_2 - E_1 - \hbar\omega_{LO}). \tag{9}$$

Here, E_2 and E_1 are the initial and final energies of the electron (hole). The square of the matrix element of electron–phonon interaction with phonon modes, localized near the interfaces, is inversely proportional to the value of the wavevector q,

$$V_q^2 \sim \frac{1}{q}. \tag{10}$$

In the balance equation for the population of electrons (holes), it is necessary to take into account the transitions to the adjacent lower level with probability $\omega \sim (N_{\rm ph} + 1)$ and to the adjacent higher level with probability $\omega \sim N_{\rm ph}$. In this case, the relaxation of an electron or hole to the bottom of the quantum well leads to the emission of dozens of optical phonons and the chain of transitions is very long. It can be shown that for an infinite chain of such levels, there are two stationary solutions. One solution describes thermodynamic equilibrium when the populations are connected by the Boltzmann relation. The second solution is dynamic, with all the populations being the same. In this case, stimulated transitions with phonon emission are compensated by stimulated transitions with phonon absorption, and the resulting rate of transitions is determined only by the probability of spontaneous transitions.

We can average (9) over all possible directions of the initial wavevector of the electron for a fixed wavevector of the phonon $\mathbf{q}$ considering $\mathbf{k}_1 = \mathbf{k}_2 - \mathbf{q}$,

$$p(\mathbf{q}) \sim \int \frac{1}{q} \delta\left(\frac{dE_1}{dk_1^2} \left(k_2^2 - 2k_2 q \cos\phi + q^2 - k_1^2 \right) \right) d\phi. \tag{11}$$

Here, $p(\mathbf{q})$ is the probability density of emitting the phonon with wavevector $\mathbf{q}$. After calculating the integral, we obtain

$$p(q) = 2\pi q p(\mathbf{q}) \sim \frac{1}{\sqrt{\left(q_p^2 - q^2\right)\left(q^2 - q_m^2\right)}}. \tag{12}$$

Here, $p(\mathbf{q})$ is the probability density to emit a phonon with wavevector equal to q, $q_m = k_2 - k_1$, $q_p = k_2 + k_1$. The proportionality factor can be found from the normalization condition by numerically calculating the integral

$$\int_{q_m}^{q_p} p(q) dq = 1. \tag{13}$$

Thus, the probability density of emitting the phonon with wavenumber q increases near the range boundaries $[k_m, k_p]$ and decreases in the middle of this range.

In order to find the density of phonon modes effectively interacting with electrons, we determine the rate of transitions of electrons near the bottom of a band accompanied by phonon absorption

$$R \sim \int \omega_q \exp\left(-\frac{E_1}{k_B T} \right) \frac{d^2 k_1}{(2\pi)^2}. \tag{14}$$

For simplicity, we consider that the electron system is nondegenerate and the second term of the integrand takes into account the Boltzmann distribution of electrons in the energy levels. We consider that $E_2 = \hbar^2 k_2^2 / 2m_c$, $E_1 = \hbar^2 k_1^2 / 2m_c$, $k_2^2 = k_1^2 + 2k_{1x}q + q^2$. After the integration, we can find the weight function, which accounts for relative contribution of different q in electron heating,

$$f_c(\mathbf{q}) = \left(\frac{2m_c \hbar\omega_{LO}}{\hbar^2 q^2} \right) \times \exp\left[-\frac{\hbar^2}{2m_c k_B T} \left(\frac{m_c \hbar\omega_{LO}}{\hbar^2 q} - \frac{q}{2} \right)^2 \right]. \tag{15}$$

A similar expression can be obtained for the holes by substituting effective mass of an electron m_c by the effective mass of a hole m_v.

The combined weight function that accounts for the relative contribution of different q in heating of both electrons and holes and be found by summing the individual taking into account the condition of charge neutrality of the QW (i.e., equal concentration of electrons and holes),

$$f_{cv}(\mathbf{q}) \sim \frac{f_c(\mathbf{q})}{m_c} + \frac{f_v(\mathbf{q})}{m_v}. \tag{16}$$

The weight function is normalized according to condition $\max f_{cv}(\mathbf{q}) = 1$. With that in mind, the density of the phonon modes which are involved in carrier thermalization near the bottom of the band can be written as

$$\rho_{\text{ph}} = \int f_{cv}(\mathbf{q}) \frac{d^2q}{(2\pi)^2}, \tag{17}$$

while the proportion of spontaneous phonons which fall into the modes involved in thermalization of the carriers near the bottom of the band is expressed as

$$\eta_{\text{ph}} = \int f_{cv}(\mathbf{q}) p(q) dq. \tag{18}$$

Note that the choice of normalization of the weight function does not affect the final result because the values ρ_{ph} and η_{ph} are found in the balance equation for non-equilibrium phonons (6) as a fraction.

The resulting approximate expression for the density of phonon modes due to the interaction of one type of the charge carriers reads as

$$\rho_{\text{ph}} = \frac{m_{\text{ph}} \sqrt{\hbar\omega_{LO} k_B T}}{\sqrt{\pi}\hbar^2}. \tag{19}$$

This expression can also be used in a general case by finding the parameter m_{ph} from numerical solution of integral (17).

As Fig. 4(a) shows, phonons intensely interacting with electrons have smaller values of wavevectors than phonons interacting with holes. This is due to the fact that effective mass of electrons is smaller than effective mass of holes. The dependence of the proportion of emitted phonons involved in carrier thermalization near the bottom of the band has a complex energy dependence determined by carrier dispersion [Fig. 4(b)]. This proportion increases near the minima of the lower subbands, but never reaches a value of 1 due to thermal distribution of the carriers. The average value of the proportion of spontaneous phonons involved in carrier thermalization at the bottom of the band is obtained by averaging over the carrier energy. In considered case, $\langle \eta_{\text{ph}} \rangle_E = 0.31$ with effective mass of the density of phonon modes $m_{\text{ph}} = 0.029$ while masses of electrons and holes are 0.050 and 0.19, respectively.

Thus, accounting for non-uniform distribution of emitted phonons along the wavevectors according to Eq. (12) and selective by wavevector interaction of electrons and holes with phonons

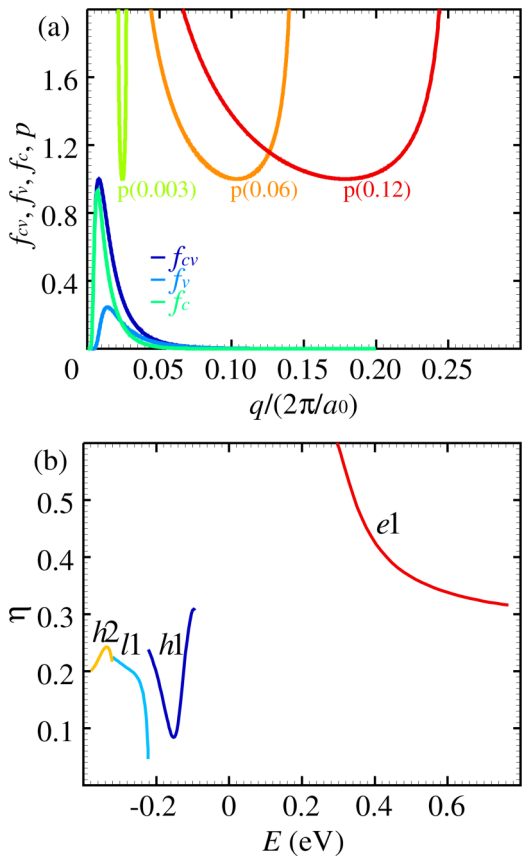

FIG. 4. (a) Dependence of the weight function for the lowest subbands of the quantum well, its electron and hole components on the wavevector of the phonon at $T = 300$ K and probability density (not normalized) of electron emitting the phonon with wavevector of $k = 0.003$, 0.06, $0.12 \times 2\pi/a_0$ (a_0—lattice constant); (b) dependence of the proportion of the emitted phonons involved in carrier thermalizations near the bottom of the band on the energy of charge carriers. Captions $e1$ denotes electron subbands, $h1$, $h2$, $l1$ denotes heavy and light hole subbands, respectively.

according to Eqs. (16)–(18) in the considered case results in 12 times higher heating rate of the non-equilibrium electron–phonon system $\eta_{\text{ph}} R/\rho_{\text{ph}}$ [see Eq. (6)] compared to the estimates obtained in the approximation of uniform distribution of emitted phonons along the wavevectors from Eq. (8).

VI. RESULTS AND DISCUSSION

One way to obtain the necessary amplification at a moderate rate of Auger recombination is to use multiple QWs instead of one. According to our calculations, $N_{\text{QW}} = 6$–10 is the optimal number of QWs, which allow to decrease Auger recombination rate with no significant increase in free carrier absorption and threshold current. The optimized current and optical confinement result in modal gain exceeding the total optical loss (estimated as 22–24 cm^{-1} at $\lambda = 3\,\mu$m in the simulated structure) up to ~350 K (Fig. 5), thus

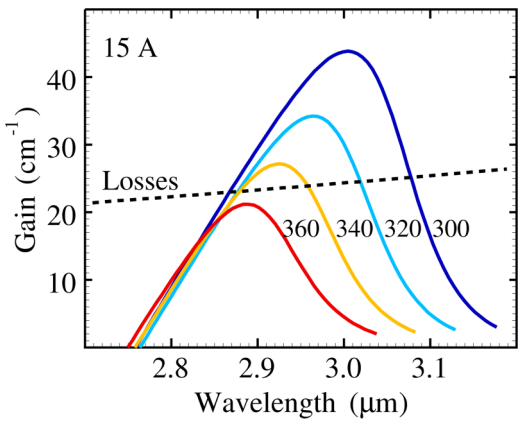

FIG. 5. Gain spectra [unsaturated: photon density $S^{(2D)} = 0$] for the TE_0 mode at lattice temperatures $T = 300$–360 K. The corresponding drive current density is $J = 15$ A. The estimated total losses are also shown with the dashed line.

allowing laser operation above room temperature. The gain maximum is shifted to shorter wavelengths with increasing temperature due to the temperature dependence of the bandgap.

The output characteristics of the laser were calculated for pulsed mode operation with 100 ns pumping current impulse. During the impulse, the active region of the structure is heated, so the momentary power and generation wavelength decrease to the end of the pulse in Fig. 6.[32] For a drive current of 16 A, the output power reduces from 1000 to 150 mW during a 100 ns pulse. With a further increase in the drive current, the power drops to zero in a time shorter than the duration of the pump pulse.

Figure 7 shows the average power, wavelength, and temperature of the active region as a function of pumping current for a 1-mm long and 100-μm wide resonator. The threshold current increases from 6 to 8 A as the number of QWs increases from 6 to

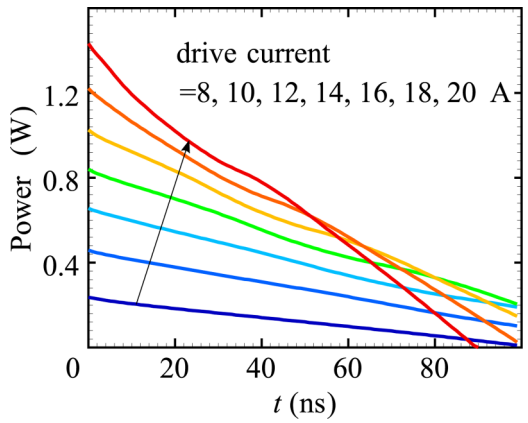

FIG. 6. Time evolution of output power of the active region during a 100 ns pulse at different drive currents. The heat sink temperature is 300 K.

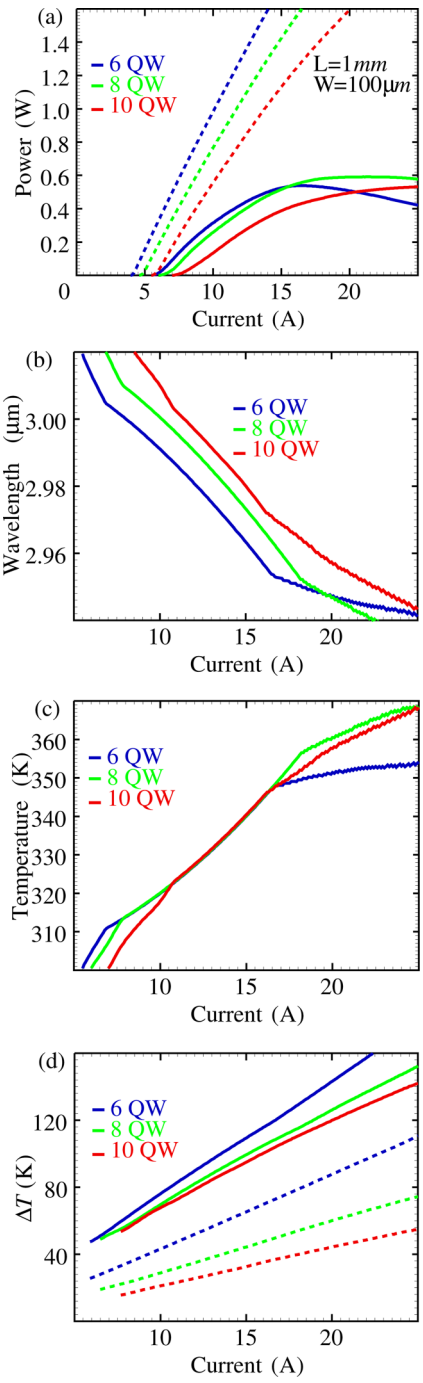

FIG. 7. Calculated (a) output power (b) lasing wavelength, (c) average temperature of the active region at the end of 100 ns pump pulse and (d) electron heating in first and last 6, 8, and 10 (dotted) QW vs drive current for resonator lengths $L = 1$ mm. Resonator width is 100 μm, reflection coefficients of the facets are $r_1 = 0.9$, $r_2 = 0.2$. The heat sink temperature is 300 K. Dashed lines in (a) correspond to calculations without taking into account the "hot" phonons effect.

10. The power 600 mW is reached at pumping current of approximately 20 A for a structure with eight wells. The threshold current density was 5.2–5.6 kA/cm^2 depending on the number of quantum wells or 0.6–0.9 kA/cm^2 per one quantum well. This falls within the range of 0.2–0.9 kA/cm^2 of the typical values of threshold current densities for type-I and type-II III-V quantum wells emitting in the same spectral range.[7] Without taking into account the effects of hot phonons, the threshold current density would be 4.8–5.2 kA/cm^2, and the output power at current of 15 A would be 1.2–2.2 W.

The calculated threshold currents of 5–6 kA/cm^2 for the proposed 3 μm interband laser are comparable with the results for QCLs based on InGaAs/AlAs(Sb)/InP[11] and InAs/AlSb.[12] The minimal threshold currents of 2 kA/cm^2 were obtained for GaInAs/AlInAs QCL with minimized leakage currents.[13] However, the interband design of the proposed laser requires much less structure layers compared to cascade lasers that reduces the requirements for long-term stability of the growth rate of molecular beam epitaxy equipment. In addition, for an interband laser, a large spectrum tuning is possible with the help of temperature (which is impossible for a QCL), that from a practical point of view is extremely convenient for tuning the radiation wavelength to absorption lines of gases.

The internal optical losses were 15, 12.5, and 10 cm^{-1} at the lasing threshold for structures with 6, 8, and 10 QWs and they increased with the pump current due to an increase in the population of QWs and waveguide layers.[58] At a current of 20 A, the internal optical losses increased to 20, 17, and 14 cm^{-1}, respectively.

The average temperature of the active region is determined by the injection current and practically does not differ for structures with different numbers of QWs [Fig. 7(c)]. The temperature averaging was performed over the time of lasing (not the entire duration of the pump, 100 ns). The kinks are related to the change in the averaging time. In the initial segment and in the final segment, the lasing duration is less than the pulse duration. In the middle segment, the lasing duration is equal to the pulse duration. The rapid increase in temperature up to the first kink is associated with an increase in the lasing duration with an increase in the pump current and the inclusion in the averaging of regions with a high temperature at the end of the pump pulse. The relatively slow temperature increase after the second kink is associated with a decrease in the lasing duration with an increase in the pump current and the exclusion from the averaging of regions with a high temperature at the end of the pump pulse. At a current of 20 A, the average heating of the active region is ~60 K. The range of the current-induced tuning of the generation wavelength is about 140 nm from ~3.02 to ~2.88 μm [Fig. 7(d)]. This tunning is related to the temperature dependence of the bandgap.

The non-equilibrium temperature of electrons and holes in the QWs was calculated using the phonon lifetime $\tau_{ph} = 0.9$ ps which was estimated from experimental data on the phonon attenuation energy.[42,59,60] At $Cd_{0.85}Hg_{0.15}Te$ barrier layers bandgap of 1.15 eV (300 K), the thermalization of each electron–hole pair to the ground QW states (separated by 0.4 eV) is accompanied by the emission of more than 40 phonons with energy of ~18 meV. Calculations have shown that accounting for the effect of "hot" phonons leads to an increase in the non-equilibrium temperature of charge carriers in the QW by 40–140 K at 20 A depending on the number of QWs. The electronic temperature in different quantum wells may strongly differ because of different current injection into these wells (the injection coefficient drops with the distance from p-emitter because of the low mobility of holes). The electron temperature decreases with the increase of the number of the QWs. Excess of electron temperature over lattice temperature about 150 K was observed experimentally.[29]

The main reason for the high threshold current is the high Auger recombination rate. When developing the design of an injection laser, it was supposed that the main Auger recombination channel is a process involving two electrons and one hole (cch).[29] Therefore, a structure with high barriers was chosen, which provided one localized level of electrons. The Auger recombination rate with the participation of electrons localized in the quantum well decreases with an increase in the barrier height due to an increase in the momentum transferred during collisions. The calculations presented in this paper showed that for the selected wavelength range, the dominant Auger recombination process is the process involving two holes and one electron (hhc), in which the final hole state is a continuum state. For this channel, suppression does not occur as the barrier height increases. Therefore, further research can be directed to the creation of a superlattice that reduces the density of hole states of the continuum in the required energy range or to use the $HgTe/Cd_{1-x}Zn_xTe$ heterosystem with deeper wells for holes. The latest strategy would yield an even more favorable valence band structure for the Auger suppression.[25] The compressively strained HgTe quantum wells grown on a $Cd_{1-x}Zn_xTe$ buffer layer would increase the energy separation between $h1/$ and $l1$ bands and provide an even greater range of energies over which the in-plane mass of the h1 holes is quite light. In addition, for better heat removal from the active region in the continuous-wave operation mode, the p-cladding CdTe layer can be reduced to the optimum thickness, at which the mode absorption in the metal contact will still be small.

VII. CONCLUSION

Thus, this paper proposes the design of an injection laser with a 2.1-nm thick HgTe QW for generation in the 3 μm region at room temperature. The analysis of structures with 6 to 10 QWs is based on a model that takes into account carrier drift and diffusion in barrier layers, capture in quantum wells, radiative and non-radiative recombination, and heating of the active region. Based on the developed technique, the refractive index of quantum-sized HgTe layers was calculated, which was 5.14 at a wavelength of 3 μm. The value of a two-dimensional Auger recombination coefficient was calculated to be 4.7×10^{-15} cm^4/s at a lattice temperature of 300 K. It is found that the contribution to the Auger recombination of transitions involving continuum states exceeds the contribution from transitions involving only localized states. The dominant mechanism of Auger recombination is a process involving two holes and one electron. A model for calculating the non-equilibrium electronic temperature due to the emission of "hot" phonons was developed. It is found that at 0.9-ps optical phonon lifetime the temperature of electrons and holes in the QW can

exceed the lattice temperature by 40–140 K depending on the number of QWs. It is shown that for structures with 8 QWs the maximum power of 600 mW is reached when pumped by 100 ns current pulses at a pumping current of 20 A, the resonator length of 1 mm, and the aperture of 100 μm. At the same time, during the pumping pulse, there is a shifting of generation wavelength of about 140 nm from ~3.02 to ~2.88 μm because of an active region lattice temperature increase of 60 K.

ACKNOWLEDGMENTS

This work was supported by the Ministry of Science and Higher Education of the Russian Federation [Grant No. 075-15-2020-797 (13.1902.21.0024)].

AUTHOR DECLARATIONS

Conflict of Interest

The authors have no conflicts to disclose.

Author Contributions

A. A. Afonenko: Conceptualization (equal); Investigation (equal); Software (equal); Writing – original draft (equal); Writing – review and editing (equal). **D. V. Ushakov:** Investigation (equal); Software (equal); Writing – original draft (equal); Writing – review and editing (equal). **A. A. Dubinov:** Investigation (equal); Writing – original draft (equal); Writing – review and editing (equal). **V. Ya. Aleshkin:** Conceptualization (equal); Investigation (equal). **S. V. Morozov:** Investigation (equal); Writing – original draft (equal). **V. I. Gavrilenko:** Conceptualization (equal); Investigation (equal); Writing – original draft (equal). **V. I. Gavrilenko:** Conceptualization (equal); Investigation (equal); Writing – original draft (equal).

DATA AVAILABILITY

The data that support the findings of this study are available from the corresponding author upon reasonable request.

REFERENCES

[1]J. Zhong, T. Mori, T. Kashiwagi, M. Yamashiro, S. Kusunose, H. Mimami, M. Tsujimoto, T. Tanaka, H. Kawashima, S. Nakagawa, J. Ito, M. Kijima, M. Iji, M. M. Watanabe, and K. Kadowaki, "Characteristic terahertz absorption spectra of paramylon and paramylonester compounds," Spectrochim. Acta Part A **244**, 118828 (2021).
[2]S. W. Sharpe, T. J. Johnson, R. L. Sams, P. M. Chu, G. C. Rhoderick, and P. A. Johnson, "Gas-phase databases for quantitative infrared spectroscopy," Appl. Spectrosc. **58**, 1452–1461 (2004).
[3]O. A. Romanovskii, S. A. Sadovnikov, O. V. Kharchenko, and S. V. Yakovlev, "Development of near/mid IR differential absorption OPO lidar system for sensing of atmospheric gases," Opt. Laser Technol. **116**, 43–47 (2019).
[4]A. Soibel, M. W. Wright, W. H. Farr, S. A. Keo, C. J. Hill, R. Q. Yang, and H. C. Liu, "Midinfrared interband cascade laser for free space optical communication," IEEE Photonics Technol. Lett. **22**, 121–123 (2010).
[5]D. Jung, S. Bank, M. L. Lee, and D. Wasserman, "Next-generation mid-infrared sources," J. Opt. **19**, 123001 (2017).
[6]G. Belenky, L. Shterengas, G. Kipshidze, and T. Hosoda, "Type-I diode lasers for spectral region above 3 μm," IEEE J. Sel. Topics Quantum Electron. **17**, 1426–1434 (2011).
[7]J. R. Meyer, C. L. Canedy, M. Kim, C. S. Kim, C. D. Merritt, W. W. Bewley, and I. Vurgaftman, "Comparison of Auger coefficients in type I and type II quantum well midwave infrared lasers," IEEE J. Quantum Electron. **57**, 2500110 (2021).
[8]J. S. Yu, A. Evans, S. Slivken, S. R. Darvish, and M. Razeghi, "Temperature dependent characteristics of $\lambda \sim 3.8\,\mu$m room-temperature continuous-wave quantum-cascade lasers," Appl. Phys. Lett. **88**, 251118–251121 (2006).
[9]S. Slivken, A. Evans, J. Nguyen, Y. Bai, P. Sung, S. R. Darvish, W. Zhang, and M. Razeghi, "Overview of quantum cascade laser research at the center for quantum devices," Proc. SPIE **6900**, 69000B1–69000B8 (2008).
[10]M. Razeghi, "High-performance InP-based mid-IR quantum cascade lasers," IEEE J. Sel. Top. Quantum Electron. **15**, 941–951 (2009).
[11]D. G. Revin, J. P. Commin, S. Y. Zhang, A. B. Krysa, K. Kennedy, and J. W. Cockburn, "InP-based midinfrared quantum cascade lasers for wavelengths below 4 μm," IEEE J. Sel. Top. Quantum Electron. **17**, 1417–1425 (2011).
[12]A. N. Baranov and R. Teissier, "Quantum cascade lasers in the InAs/AlSb material system," IEEE J. Sel. Top. Quantum Electron. **21**, 85–95 (2015).
[13]N. Bandyopadhyay, Y. Bai, S. Tsao, S. Nida, S. Slivken, and M. Razeghi, "Room temperature continuous wave operation of $\lambda \sim 3$–$3.2\,\mu$m quantum cascade lasers," Appl. Phys. Lett. **101**, 241110 (2012).
[14]D. G. Revin, J. W. Cockburn, M. J. Steer, R. J. Airey, M. Hopkinson, A. B. Krysa, L. R. Wilson, and S. Menzel, "InGaAs/AlAsSb/InP quantum cascade lasers operating at wavelengths close to 3 μm," Appl. Phys. Lett. **90**, 021108 (2007).
[15]J. P. Commin, D. G. Revin, S. Y. Zhang, A. B. Krysa, K. Kennedy, and J. W. Cockburn, "High peak power $\lambda \sim 3.3$ and $3.5\,\mu$ InGaAs/AlAs(Sb) quantum cascade lasers operating up to 400 K," Appl. Phys. Lett. **97**, 031108 (2010).
[16]O. Cathabard, R. Teissier, J. Devenson, J. C. Moreno, and A. N. Baranov, "Quantum cascade lasers emitting near 2.6 μm," Appl. Phys. Lett. **96**, 141110 (2010).
[17]A. Rogalski, "HgCdTe infrared detector material: History, status and outlook," Rep. Prog. Phys. **68**, 2267–2336 (2005).
[18]A. Singh, V. Srivastav, and R. Pal, "HgCdTe avalanche photodiodes: A review," Opt. Laser Technol. **43**, 1358–1370 (2011).
[19]I. Melngailis and A. J. Strauss, "Spontaneous and coherent photoluminescence in $Cd_xHg_{1-x}Te$," Appl. Phys. Lett. **8**, 179–180 (1966).
[20]J. M. Arias, M. Zandian, R. Zucca, and J. Singh, "HgCdTe infrared diode lasers grown by MBE," Semicond. Sci. Technol. **8**, S255–S260 (1993).
[21]A. Million, T. Colin, P. Ferret, J. P. Zanatta, P. Bouchut, G. L. Destefanis, and J. Bablet, "HgCdTe double heterostructure for infrared injection laser," J. Cryst. Growth **127**, 291–295 (1993).
[22]H. Q. Le, J. M. Arias, M. Zandian, R. Zucca, and Y. Z. Liu, "High-power diode-laser-pumped midwave infrared HgCdTe/CdZnTe quantum-well lasers," Appl. Phys. Lett. **65**, 810–812 (1994).
[23]J. Bonnet-Gamard, J. Bleuse, N. Magnea, and J. L. Pautrat, "Optical gain and laser emission in HgCdTe heterostructures," J. Appl. Phys. **78**, 6908–6915 (1995).
[24]J. Bonnet-Gamard, J. Bleuse, N. Magnea, and J. L. Pautrat, "Emission wavelength and cavity design dependence of laser behaviour in HgCdTe heterostructures," J. Cryst. Growth **159**, 613–617 (1996).
[25]I. Vurgaftman and J. R. Meyer, "High-temperature HgTe/CdTe multiple-quantum-well lasers," Opt. Exp. **2**, 137–142 (1998).
[26]G. Alymov, V. Vyurkov, V. Ryzhii, A. Satou, and D. Svintsov, "Auger recombination in Dirac materials: A tangle of many-body effects," Phys. Rev. B **97**, 205411 (2018).
[27]V. Y. Aleshkin, A. A. Dubinov, V. V. Rumyantsev, and S. V. Morozov, "Threshold energies of Auger recombination in HgTe/CdHgTe quantum well heterostructures with 30–70 meV bandgap," J. Phys.: Condens. Matter **31**, 425301 (2019).
[28]G. Alymov, V. Rumyantsev, S. Morozov, V. Gavrilenko, V. Aleshkin, and D. Svintsov, "Fundamental limits to far-infrared lasing in Auger-suppressed HgCdTe quantum wells," ACS Photonics **7**, 98–104 (2020).
[29]K. E. Kudryavtsev, V. V. Rumyantsev, V. Y. Aleshkin, A. A. Dubinov, V. V. Utochkin, M. A. Fadeev, N. N. Mikhailov, G. Alymov, D. Svintsov,

V. I. Gavrilenko, and S. V. Morozov, "Temperature limitations for stimulated emission in 3–4 μm range due to threshold and non-threshold Auger recombination in HgTe/CdHgTe quantum wells," Appl. Phys. Lett. **117**, 083103 (2020).
[30]M. A. Fadeev, V. V. Rumyantsev, A. M. Kadykov, A. A. Dubinov, A. V. Antonov, K. E. Kudryavtsev, S. A. Dvoretskii, N. N. Mikhailov, V. I. Gavrilenko, and S. V. Morozov, "Stimulated emission in 2.8–3.5 μm wavelength range from Peltier cooled HgTe/CdHgTe quantum well heterostructures," Opt. Exp. **26**, 12755–12760 (2018).
[31]M. A. Fadeev, A. O. Troshkin, A. A. Dubinov, V. V. Utochkin, A. A. Razova, V. V. Rumyantsev, V. Y. Aleshkin, V. I. Gavrilenko, N. N. Mikhailov, S. A. Dvoretsky, and S. V. Morozov, "Mid IR stimulated emission in HgCdTe/CdHgTe quantum well heterostructures at room temperature," Opt. Eng. **60**, 082006 (2021).
[32]A. Afonenko, D. Ushakov, G. Alymov, A. Dubinov, S. Morozov, V. Gavrilenko, and D. Svintsov, "Feasibility of lasing in the GaAs Reststrahlen band with HgTe multiple quantum well laser diodes," J. Phys. D: Appl. Phys. **54**, 175108 (2021).
[33]D. Ushakov, A. Afonenko, R. Khabibullin, D. Ponomarev, V. Aleshkin, S. Morozov, and A. Dubinov, "HgCdTe-based quantum cascade lasers operating in the GaAs phonon Reststrahlen band predicted by the balance equation method," Opt. Exp. **28**, 25371–25382 (2020).
[34]V. V. Utochkin, V. Y. Aleshkin, A. A. Dubinov, V. I. Gavrilenko, N. S. Kulikov, M. A. Fadeev, V. V. Rumyantsev, N. N. Mikhailov, S. A. Dvoretsky, A. A. Razova, and S. V. Morozov, "Continuous-wave stimulated emission in the 10–14-μm range under optical excitation in HgCdTe/CdHgTe-QW structures with quasirelativistic dispersion," Semiconductors **54**, 1371–1375 (2020).
[35]V. S. Evstigneev, A. V. Chilyasov, A. N. Moiseev, S. V. Morozov, and D. I. Kuritsyn, "Arsenic doping upon the deposition of CdTe layers from dimethylcadmium and diisopropyltellurium," Semiconductors **55**, 7–13 (2021).
[36]E. G. Novik, A. Pfeuffer-Jeschke, T. Jungwirth, V. Latussek, C. R. Becker, G. Landwehr, H. Buhmann, and L. W. Molenkamp, "Band structure of semimagnetic $Hg_{1-y}Mn_yTe$ quantum wells," Phys. Rev. B **72**, 035321 (2005).
[37]V. Y. Aleshkin and A. A. Dubinov, "Effect of the spin orbit interaction on intersubband electron transition in GaAs/AlGaAs quantum well heterostructures," Phys. B **503**, 32–37 (2016).
[38]W. Scott, "Electron mobility in $Hg_{1-x}Cd_xTe$," J. Appl. Phys. **43**, 1055–1062 (1972).
[39]A. Nagaoka, D. Kuciauskas, J. McCoy, and M. A. Scarpulla, "High p-type doping, mobility, photocarrier lifetime in arsenic-doped CdTe single crystals," Appl. Phys. Lett. **112**, 192101 (2018).
[40]J. A. Mroczkowski and D. A. Nelson, "Optical absorption below the absorption edge in $Hg_{1-x}Cd_xTe$," J. Appl. Phys. **54**, 2041–2051 (1983).
[41]J. P. Laurenti, J. Camassel, A. Bouhemadou, B. Toulouse, R. Legros, and A. Lusson, "Temperature dependence of the fundamental absorption edge of mercury cadmium telluride," J. Appl. Phys. **67**, 6454–6460 (1990).
[42]M. Grynberg, R. Le Toullec, and M. Balkanski, "Dielectric function in HgTe between 8 and 300 K," Phys. Rev. B **9**, 517–526 (1974).
[43]C. G. Van de Walle, "Band lineups and deformation potentials in the model-solid theory," Phys. Rev. B **39**, 1871–1883 (1989).
[44]Z. Kučera, "Dispersion of the refractive index of $Hg_{1-x}Cd_xTe$," Phys. Stat. Sol. A **100**, 659–665 (1987).
[45]A. N. Pikhtin and A. D. Yas'kov, "Disperson of the refractive index of semiconductors with diamond and zinc-blende structures," Sov. Phys. Semicond. **12**, 622–626 (1978).
[46]S. Adachi, "Model dielectric constants of GaP, GaAs, GaSb, InP, InAs, InSb," Phys. Rev. B **35**, 7454–7463 (1987).
[47]E. D. Palik, *Handbook of Optical Constants of Solids* (Academic Press, 1998), p. 999.
[48]C. E. Jones, T. N. Casselman, J. P. Faurie, S. Perkowitz, and J. N. Schulman, "Infrared properties and band gaps of HgTe/CdTe superlattices," Appl. Phys. Lett. **47**, 140–142 (1985).
[49]A. A. Afonenko and D. V. Ushakov, "Current-injection efficiency in semiconductor lasers with a waveguide based on quantum wells," Semiconductors **48**, 83–88 (2014).
[50]A. R. Beattie and P. T. Landsberg, "Auger effect in semiconductors," Proc. R. Soc. London A **249**, 16–29 (1959).
[51]Y. Jiang, M. C. Teich, and W. I. Wang, "Carrier lifetimes and threshold currents in HgCdTe double heterostructure and multiquantum-well lasers," J. Appl. Phys. **69**, 6869–6875 (1991).
[52]A. S. Polkovnikov and G. G. Zegrya, "Auger recombination in semiconductor quantum wells," Phys. Rev. B **58**, 4039–4056 (1998).
[53]L. V. Asryan, N. A. Gun'ko, A. S. Polkovnikov, G. G. Zegrya, R. A. Suris, P.-K. Lau, and T. Makino, "Threshold characteristics of InGaAsP/InP multiple quantum well lasers," Semicond. Sci. Technol. **15**, 1131–1140 (2000).
[54]S. O. Slipchenko, Z. N. Sokolova, N. A. Pikhtin, K. S. Borschev, D. A. Vinokurov, and I. S. Tarasov, "Finite energy scattering time of charge carriers as an origin of optical power limitation in semiconductor lasers," Semiconductors **40**, 1017–1023 (2006).
[55]D. A. Firsov, L. Shterengas, G. Kipshidze, V. L. Zerova, T. Hosoda, P. Thumrongsilapa, L. E. Vorobjev, and G. Belenky, "Dynamics of photoluminescence and recombination processes in Sb-containing laser nanostructures," Semiconductors **44**, 53–61 (2010).
[56]B. K. Ridley, "Hot electrons in low-dimensional structures," Rep. Prog. Phys. **54**, 169–256 (1991).
[57]E. Ozturk, A. Straw, N. Balkan, G. Jones, J. Frost, and D. Ritchie, "Energy and momentum relaxation of hot electrons in $GaAs/AI_xGa_{1-x}As$ quantum wells: Effect of hot phonon lifetime," Semicond. Sci. Technol. **7**, 1417–1421 (1992).
[58]Z. N. Sokolova, D. A. Veselov, N. A. Pikhtin, I. S. Tarasov, and L. V. Asryan, "Increase in the internal optical loss with increasing pump current and the output power of quantum well lasers," Semiconductors **51**, 959 (2017).
[59]Q. Dingrong, "Far-infrared reflectivity: A novel tool in the investigation of the relaxation process of excess carriers in HgCdTe," J. Appl. Phys. **70**, 7191–7193 (1991).
[60]D. N. Talwar, T.-R. Yang, Z. C. Feng, and P. Becla, "Infrared reflectance and transmission spectra in II-VI alloys and superlattices," Phys. Rev. B **84**, 174203 (2011).